AFRL-RY-WP-TR-2020-0004

A BOUNDARY LAYER MODEL FOR UNBOUNDED FLOW ALONG A WALL

David Weyburne

Optoelectronics Technology Branch
Aerospace Components & Subsystems Division

FEBRUARY 2020
Final Report

AIR FORCE RESEARCH LABORATORY
SENSORS DIRECTORATE
WRIGHT-PATTERSON AIR FORCE BASE, OH 45433-7320
AIR FORCE MATERIEL COMMAND
UNITED STATES AIR FORCE

NOTICE AND SIGNATURE PAGE

Using Government drawings, specifications, or other data included in this document for any purpose other than Government procurement does not in any way obligate the U.S. Government. The fact that the Government formulated or supplied the drawings, specifications, or other data does not license the holder or any other person or corporation; or convey any rights or permission to manufacture, use, or sell any patented invention that may relate to them.

This report was cleared for public release by the USAF 88th Air Base Wing (88 ABW) Public Affairs Office (PAO) and is available to the general public, including foreign nationals. Copies may be obtained from the Defense Technical Information Center (DTIC) (http://www.dtic.mil).

AFRL-RY-WP-TR-2020-0004 HAS BEEN REVIEWED AND IS APPROVED FOR PUBLICATION IN ACCORDANCE WITH ASSIGNED DISTRIBUTION STATEMENT.

// Signature//	// Signature//
DAVID T. TOMICH, Program Manager Optoelectronics Technology Branch Aerospace Components & Subsystems Division	FRED E. ARNOLD, Branch Chief Optoelectronics Technology Branch Aerospace Components & Subsystems Division

This report is published in the interest of scientific and technical information exchange, and its publication does not constitute the Government's approval or disapproval of its ideas or findings.

*Disseminated copies will show "//Signature//" stamped or typed above the signature blocks.

REPORT DOCUMENTATION PAGE

Form Approved
OMB No. 0704-0188

1. REPORT DATE *(DD-MM-YY)*	2. REPORT TYPE	3. DATES COVERED *(From - To)*
February 2020	Final	1 November 2014 – 13 April 2015

4. TITLE AND SUBTITLE
A BOUNDARY LAYER MODEL FOR UNBOUNDED FLOW ALONG A WALL

5a. CONTRACT NUMBER
In-house

5b. GRANT NUMBER

5c. PROGRAM ELEMENT NUMBER
N/A

6. AUTHOR(S)
David Weyburne

5d. PROJECT NUMBER
N/A

5e. TASK NUMBER
N/A

5f. WORK UNIT NUMBER
N/A

7. PERFORMING ORGANIZATION NAME(S) AND ADDRESS(ES)

Optoelectronics Technology Branch
Aerospace Components & Subsystems Division
Air Force Research Laboratory, Sensors Directorate
Wright-Patterson Air Force Base, OH 45433-7320
Air Force Materiel Command, United States Air Force

8. PERFORMING ORGANIZATION REPORT NUMBER
AFRL-RY-WP-TR-2020-0004

9. SPONSORING/MONITORING AGENCY NAME(S) AND ADDRESS(ES)

Air Force Research Laboratory
Sensors Directorate
Wright-Patterson Air Force Base, OH
45433-7320
Air Force Materiel Command
United States Air Force

Air Force Office of Scientific
Research Public Affairs (AFOSR)
875 North Randolph Street
Suite 325, Room 3112
Arlington, VA 22203

10. SPONSORING/MONITORING AGENCY ACRONYM(S)
AFRL/RYDH

11. SPONSORING/MONITORING AGENCY REPORT NUMBER(S)
AFRL-RY-WP-TR-2020-0004

12. DISTRIBUTION/AVAILABILITY STATEMENT
Approved for public release; distribution is unlimited.

13. SUPPLEMENTARY NOTES
PAO Case Number 88ABW-2020-0072, Clearance Date 9 January 2020. Report contains color.

14. ABSTRACT
The current boundary layer model used in describing flow along a wall is found to be incomplete in that it only describes the flow found in a wind tunnel. The important attribute of the wind tunnel case is that the velocity above the wall asymptotes to a constant value that is different than the free stream inlet velocity. In contrast, for flows along an airfoil, the velocity above the airfoil surface must eventually return to the free stream inlet flow velocity value. Hence, a new boundary layer model is required for this case. Herein, we define a new region above the viscous layer as the inertial boundary layer region. New thickness and shape parameters are defined and similarity solutions are proposed.

15. SUBJECT TERMS
boundary layer theory, unbounded flow, boundary layer thickness, inertial boundary layer, moment method, airfoil

16. SECURITY CLASSIFICATION OF:			17. LIMITATION OF ABSTRACT:	18. NUMBER OF PAGES	19a. NAME OF RESPONSIBLE PERSON (Monitor)
a. REPORT	b. ABSTRACT	c. THIS PAGE			David Tomich
Unclassified	Unclassified	Unclassified	SAR	35	19b. TELEPHONE NUMBER *(Include Area Code)* N/A

Table of Contents

Section **Page**

List of Figures

Figure **Page**

1. SUMMARY

The traditional boundary layer model used in describing laminar and turbulent flow along a wall does not work for unbounded flow along a wall or airfoil. The traditional boundary layer model only describes the flow that is normally obtained in a wind tunnel or a two-dimensional (2-D) closed channel with a large gap separation. For these cases, the boundary layer is considered to be the region bounded by the boundary layer edge where the boundary layer edge is defined as the point above the plate where the velocity in the flow direction asymptotes to a velocity that, in general, is different than the inlet free stream velocity. However, for flow along a plate without an upper or lower wall boundary, this model does not work. For unbounded flows, the flow above the traditional viscous boundary layer must gradually return to the free stream inlet velocity value. To correct this deficiency, we define a new boundary layer model for the unbounded case. The main feature of the new model is a new region located just above the traditional viscous boundary layer region. We call this new region the inertial boundary layer region since viscous affects are mostly absent. Using the moment method approach, new thickness and shape parameters are defined to describe this region. The new model is demonstrated by applying it to computer simulation results for air flow over a NACA0012 airfoil. The boundary layer thickness for the inertial boundary layer region is calculated to be about 10 cords for a flow with 0.5 Mach inlet flow velocity. This means the traditional viscous boundary layer thickness is only about 0.5% of the total boundary layer thickness for flow along an airfoil. It is shown that this new region has similarity solutions to the flow governing equations. This means that it should be possible to cobble together a complete theory for lift/drag on an airfoil using the new boundary layer model.

2. INTRODUCTION

The boundary layer concept was first developed by Ludwig Prandtl[1] as a means to describe fluid flow along a wall. The traditional interpretation of this concept for 2-D flow is depicted in Fig. 1 for laminar flow along a flat plate at zero-degree inclination (assume the flow and the plate extends to infinity in the positive/negative direction perpendicular to the *x*-*y* plane). The velocity profile is defined as the velocity $u(x, y)$ viewed in the direction normal to the wall at a point x for all y where $u(x, y)$ is the velocity in the flow direction along the wall. Due to viscosity effects, the velocity at the wall surface is zero and gradually increases until it asymptotes at the boundary layer edge to $u_e(x)$. The boundary layer thickness, $\delta(x)$, (dashed line) is described as the point where the velocity $u(x, y)$ reaches the asymptotic boundary layer edge velocity $u_e(x)$. The traditional boundary layer description has worked well for the past 100 years. Velocity profiles similar to those depicted in Fig. 1 are routinely measured in wind tunnels around the world. Many traditional wind tunnels all have a common feature in their implementation that allows the pressure gradient in the flow direction to be manipulated by adjusting the upper surface height of the wind tunnel. Indeed, in most wind tunnels, one can construct flows along the plate with a zero-pressure gradient (ZPG), a favorable pressure gradient (FPG), and an adverse pressure gradient (APG) by adjusting the ceiling height along the flow direction. For what seems to be expediency, the traditional depiction in Fig. 1 has not included the presence of the upper wall or some indication of the presence of the upper surface pressure gradient due to the upper wall. Hence, the traditional depiction of what one would expect for flow along a wall in a wind tunnel is not complete. When the boundary layer along the plate interacts with the top surface's boundary layer then what we have is 2-D channel flow with a large gad separation. This is what appears to be the case in most wind tunnel experiments.

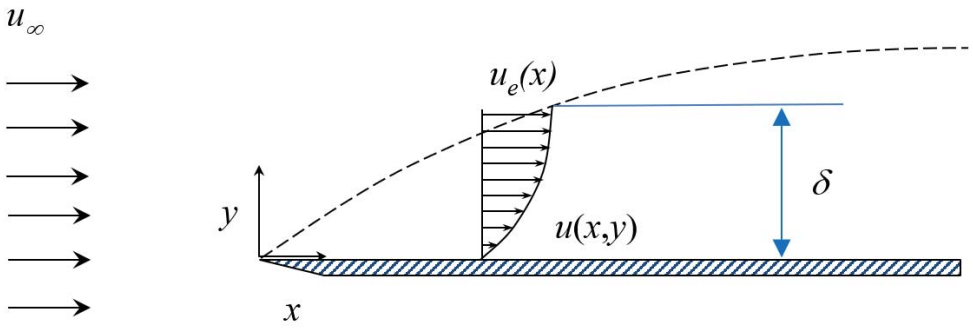

Figure 1: The Traditional, but incomplete, Rendering of 2D Laminar Boundary Layer Flow over a Semi-infinite Flat Plate

The boundary layer story becomes more complicated for the case of airflow over an airfoil. What is depicted in Fig. 1 is not what one would expect for flow over a plate-airfoil in an unbounded uniformly moving airmass. For what we will call the "unbounded boundary layer" case, the velocity normal to the airfoil must eventually return to this free stream velocity at some point above the plate-airfoil. This means that the boundary layer does not stop at the traditional viscous boundary layer edge but continues until the velocity above the plate returns to the free

stream inlet flow velocity u_∞. Thus, the traditional boundary layer model depicted in Fig. 1 is also not correct for a plate-airfoil in an unbounded uniformly moving airmass. In what follows, we remedy the situation by adding a second region above the traditional viscous boundary layer region. We call this the inertial boundary layer region since viscous forces are mostly absent. The new model for flow along a plate-airfoil is depicted in Fig. 2. The boundary layer thickness next to the plate-airfoil becomes $\delta_{\max}$ and this region is characterized by the presence of viscous effects. Above this region, the new inertial boundary layer is characterized by the thickness δ_i such that above δ_i the velocity is essentially the free steam velocity u_∞. These terms will be explored in more detail below. What is NOT shown in Fig. 2 is the case for turbulent boundary layer flow on an airfoil. What we can say is that if turbulence is present than an additional region would be needed to be added between the viscous and inertial boundary layer regions at some point along the plate. For clarity, we will ignore the turbulent region for now.

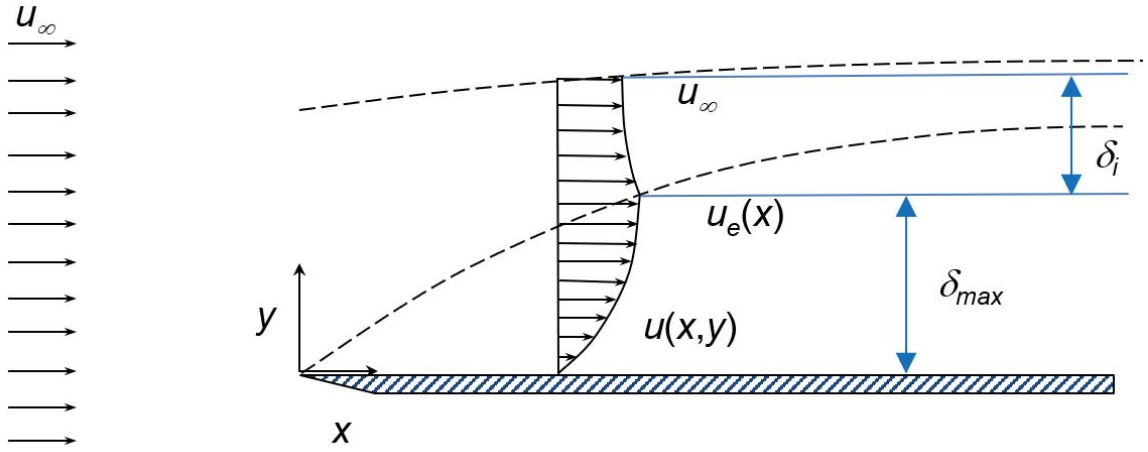

Figure 2: Schematic Drawing depicting new Model for Laminar Flow over a Plate Airfoil

Drawing is not to scale since, in general, $\delta_i >> \delta_{\max}$.

In order to mathematically describe the new unbounded boundary layer inertial region, we will adopt the central moment method developed by Weyburne[2,3] for mathematically describing the thickness and shape of the tradition wind tunnel boundary layer. In those papers, it was found that laminar and turbulent boundary layers along a wall in a wind tunnel could be described by the central moment method traditionally used in statistical analysis to describe a random variables probability distribution. With the moment method, Weyburne[3] showed that it is possible to describe both the outer inertial turbulent region and the inner viscous region of a turbulent boundary layer flow along a wall using simple integrals of the velocity profile. It was found that the ratio of the turbulent boundary layer outer region thickness to the viscous boundary layer inner thickness ranged from 4-5 at low Reynolds number to something like 35 at high Reynolds number.[3] In contrast, in what follows, we show that the thickness ratio of the inertial region to the viscous region for laminar flow along an airfoil is more like 200 for the laminar flow case. The main reason for this appears to be very slow decay of the peak velocity to the free stream flow velocity.

In what follows, we undertake a full description for laminar flow over a plate-airfoil in an unbounded moving airmass. This includes not only a physical description based on the moment method but also a look at the behavior of the plate-airfoil boundary layer as it pertains to theoretical solutions to the flow governing equations. We show that the new inertial boundary layer is amendable to similarity solutions.

3. VELOCITY PROFILE BOUNDARY LAYER MODEL

3.1 Large Gap 2-D Channel Model

A boundary layer model needs to describe the behavior of the velocity profile as one moves down the wall in the flow direction. The model for boundary layer flow along a wall is often depicted as shown in Fig. 1. The no-slip boundary condition at the wall means that the velocity at the wall is zero. The velocity profile monotonically increases to a velocity at the boundary layer edge at which point the velocity asymptotes to a velocity $u_e(x)$. This boundary layer edge velocity $u_e(x)$ changes along the wall depending on the pressure gradient along the wall in the flow direction. The boundary layer thickness $\delta(x)$ is considered to be the point where the velocity reaches the asymptotic velocity at the boundary layer edge $u_e(x)$. The boundary layer quantities like the displacement thickness and momentum thickness are all calculated relative to this boundary layer edge velocity. Although not usually acknowledged as a 2-D channel model with a large gap separation, this is the model that has been used since the introduction of the boundary layer concept by Ludwig Prandtl[1] over a hundred years ago.

3.2 Proposed New Unbounded Boundary Layer Model

The description above applies to flow normally encountered in most wind tunnels. However, for flow over a plate-airfoil in an unbounded moving airmass, this model does not work. For the unbounded case, the velocity normal to the plate-airfoil must eventually return to this free stream inlet velocity u_∞ at some point above the plate-airfoil. This means that the boundary layer does not end at the traditional boundary layer edge but continues until the velocity above the plate returns to the free stream inlet flow velocity. Hence, the boundary layer does NOT end at the point where the viscous (or turbulent) effects are absent. There has to be a region further out from the viscous (or turbulent) boundary layer edge where the velocity returns to the free stream velocity u_∞. We will refer to this region as the inertial boundary layer region since in this region the viscous contributions are mostly absent.

The boundary layer model depicted in Fig. 2 can be demonstrated by examining computer simulation results. In Fig. 3 we show the 4096 by 2048 mesh simulation result for the *x*-velocity (flow direction) around a NACA0012 airfoil obtained by Swanson and Langer.[4] The flow corresponds to the full Navier-Stokes compressible (mostly laminar flow) case with a small amount of trailing edge separation beginning at approximately the *x/c*=0.8 (*c* is the cord length).

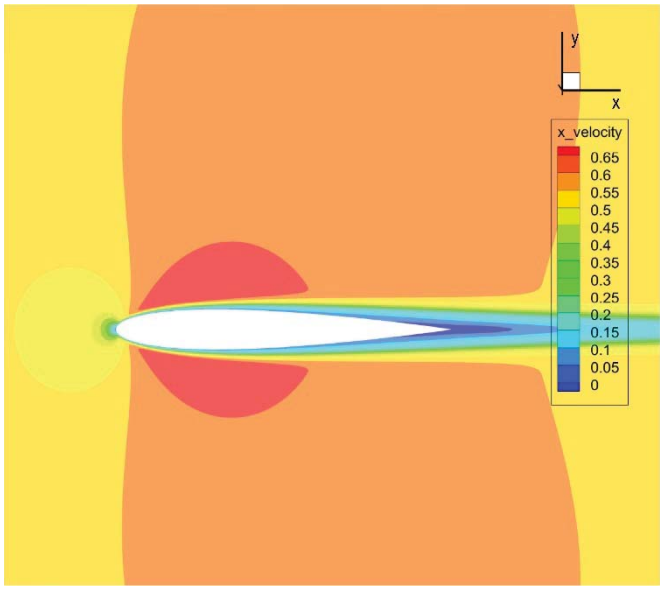

Figure 3: Swanson and Langer[4] 2-D Simulation of Laminar Flow over a NACA0012 Wing with M = 0.5, α = 0, and Re = 5000

The flow conditions are Mach (M)= 0.5, airfoil inclination angle $\alpha = 0$, and Re =5000. In Fig. 4a we show a normal to the wall velocity profile (x-direction velocity looking in the y-direction) taken at x/c = 0.3. In Fig. 4b we show the same profile but using a logarithmic scale. In Fig. 4b we also show a number of relevant thickness markers. The maximum $u(x, y)$ profile value given by $u_{\max}$ is located at $\delta_{\max}$. It is a thickness measure that we will show below that is related to the viscous boundary layer thickness. It will be used interchangeably with the viscous boundary layer thickness δ_v which has a directly identifiable relation to the physics of the flow. The δ_i value is the inertial boundary layer thickness value. It is evident from Fig. 4b that the inertial thickness is much larger than $\delta_{\max}$ (or δ_v). For the example shown in Fig. 4, the ratio δ_i / δ_v is about 220. It is a given that, in general, $\delta_{\max}$, δ_i, and δ_v change with the distance along the wing cord x/c.

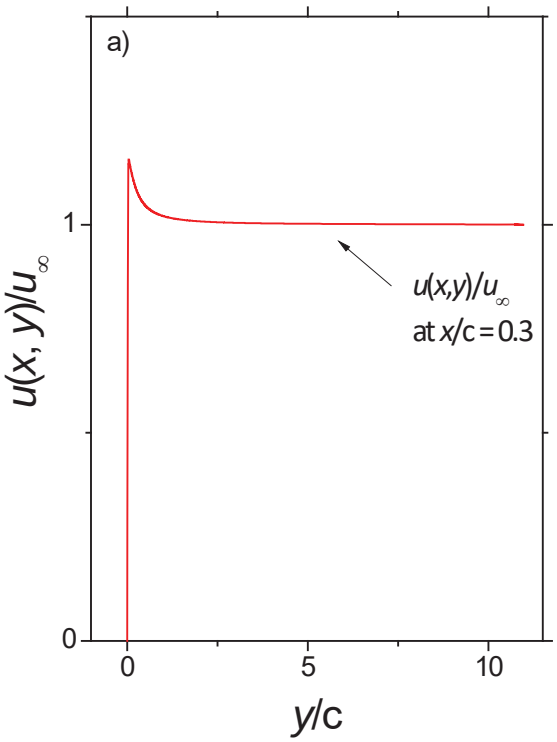

Figure 4a: Velocity Profile Normal to the Airfoil at x/c = 0.3 from Swanson and Langer[4]

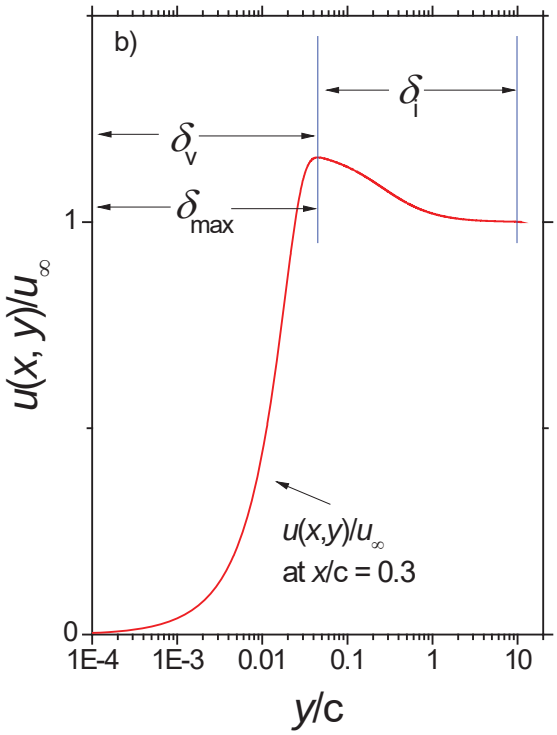

Figure 4b: Same as Figure 4a but with a Log Scale

δ_l, δ_v, and δ_{max} are the length scales

3.2.1 Calculating δ_{max} and δ_v

Determining the value of δ_{max} is straightforward and needs no further explanation.

Weyburne[2] developed the viscous boundary layer thickness δ_v concept based on the viscous term of the *x*-momentum conservation equation. The viscous forces will only contribute to the overall flow momentum when the second derivative of the velocity is significant. This led to the viscous boundary layer being defined in terms of central moments of the negative of the second derivative of $u(x, y)$. The reasoning behind the use of the central moments was the observation that the second derivative of the Blasius[5] laminar boundary layer had a distinctly Gaussian-like appearance.[2] It therefore makes sense to adopt the moment method used to describe probability density functions for this case.

However, in looking at some of the second derivatives of the velocity profiles for the NACA0012 airfoil, we found that the APG region (~*x/c*=0.3 to ~*x/c*=0.8) had noticeable nonprobability density function like behavior in that the near wall region takes on negative values. An example is plotted in Fig. 5a for the profile at *x/c*=0.5 (note that the moment method is based on the negative of the second derivative). Probability density functions cannot take on negative values. This negative behavior observed in Fig. 5a means that the standard moment method for the viscous region employed by Weyburne[2,3] for ZPG cases will not work for the APG cases.

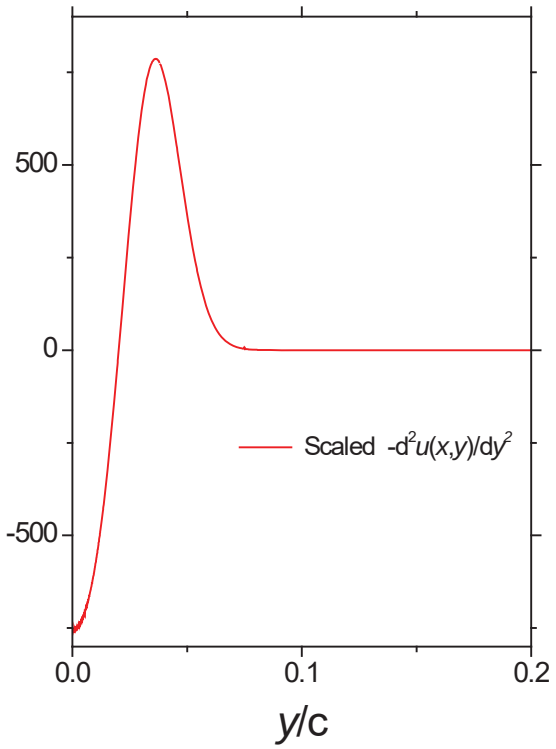

Figure 5a: Scaled Second Derivative of the *x*-velocity at *x/c*=0.5

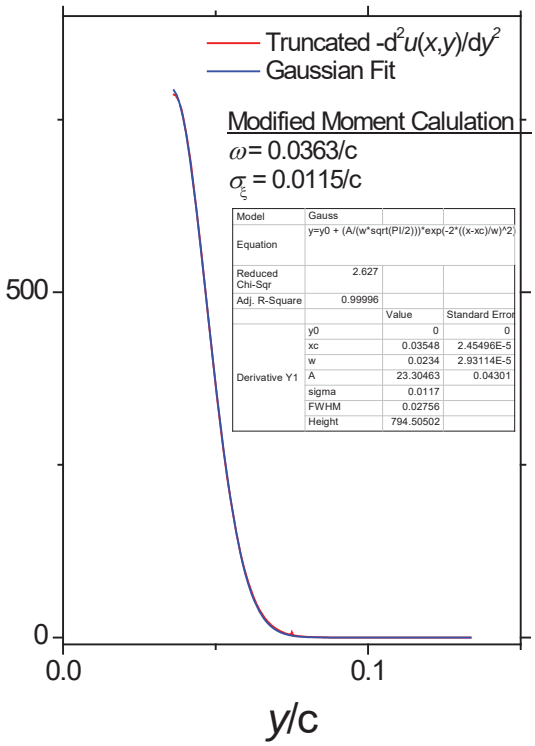

Figure 5b: A Gaussian Fit to the truncated Second Derivative Data at *x/c*=0.5

It will not work in the sense that the calculated boundary layer thickness will not correctly identify the point where the viscous forces are no longer significant. By observing Fig. 5a, it is apparent that a simple work around for the APG cases is to just ignore the second derivative data for *y/c* less than second derivative maximum located at about *y/c* = 0.036 for the *x/c*=0.5 case (note that the *y/c*=0 corresponds to the airfoil surface). The result of the truncation is shown in Fig. 5b. This leaves us with a proper probability density function like curve. We can therefore modify the standard moment method and define the viscous velocity boundary layer *n*th central moment, ζ_n for APG based wall-bounded 2-D laminar flow over an airfoil as

$$\zeta_n = -\frac{1}{\alpha}\int_{\omega}^{h} dy\,(y-\omega)^n \frac{d^2u(x,y)}{dy^2} \quad , \tag{1}$$

where *y*=*h* is deep into the free stream, where we take ω as the *y*-value at the second derivatives negative maximum, and where the normalizing parameter is

$$\alpha = -\int_{\omega}^{h} dy \frac{d^2u(x,y)}{dy^2} \quad . \tag{2}$$

The viscous boundary layer width, σ_ζ, is defined in terms of the second central moment as $\sigma_\zeta = 2\sqrt{\zeta_2}$. The four-sigma viscous boundary layer thickness δ_v is then defined as $\delta_v = \omega + 4\sigma_\zeta$. For the curve in Fig. 5b, the estimated the four-sigma viscous boundary layer thickness is $\delta_v = 0.0815/c$. The central moments can be used to define shape parameters based on the third and fourth moments in a fashion similar to the method described by Weyburne.[3] Although primarily intended for the APG region, the above method should work for the ZPG and FPG regions as well.

The physics of this truncated second derivative region in Fig. 5b is interesting. We found that the Gaussian-like behavior observed for the ZPG case[2] also applies in this truncated APG region. As confirmation, we show the Gaussian fit to the truncated section in Fig. 5b. The fit is excellent with an adjusted R squared value of 0.9996. The fit essentially overlaps the experimental data. The σ_ζ (= *sigma*) values from the fit are a close match to the Eq. 1 moment-based values (see Fig. 5b inset).

The viscous thickness δ_v is easily calculated for simulation data where high quality second derivative data is readily available. That is not the case for wind tunnel type experimental data, in general, where experimental measurement noise can make the second derivative data unusable. Weyburne[3] also showed that δ_v can be determined if the skin friction is known or measurable. However, this option does not seem to be something easily accomplished in an airfoil experiment. This makes determining δ_v for the non-computer-based airfoil case problematic. Given the problem of calculating δ_v, we examine $\delta_{\max}$ as a possible substitute. The computer simulation data allows us to examine both quantities. We found that the maximum velocity located at $\delta_{\max}$ correlates well with the 2.6 sigma thickness given by $\delta_v^{2.6} = \omega + 2.6\,\sigma_\zeta$. This result is illustrated in Fig. 6 for a range of *x*/*c* values spanning most of the airfoils cord. The correlation is only slightly worse in the vicinity of the trailing edge separation point. The implication of this result is that $u_{\max}(x)$ is a reasonable substitute for the boundary layer edge velocity $u_e(x)$ and $\delta_{\max}(x)$ is a reasonable substitute for $\delta_v(x)$.

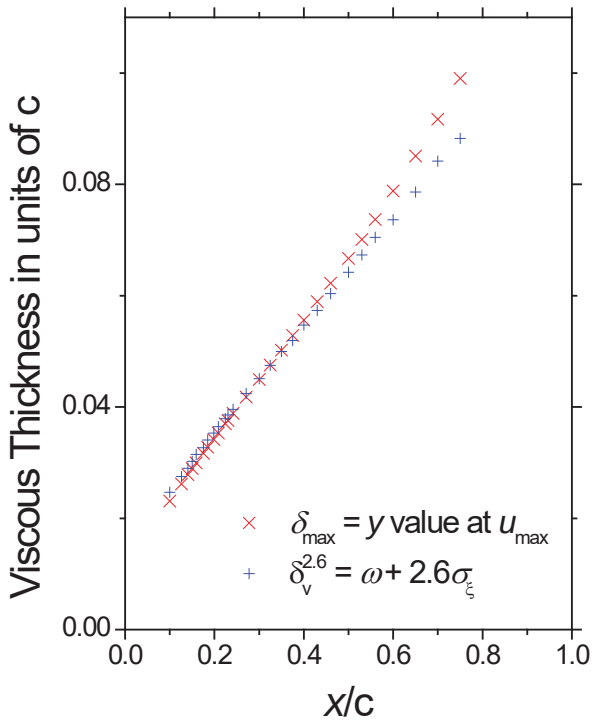

Figure 6: The Viscous Boundary Layer Thickness compared to the Maximum Thickness Location

The displacement thickness for the viscous region can be defined in a number of ways. For simplicity, we choose to define the displacement thickness as

$$\delta_1^v = \int_0^{\delta_v} dy \left(1 - \frac{u(x,y)}{u_e(x)}\right) \quad . \tag{3}$$

For cases where δ_v is not easily calculated, then $\delta_{\max}$ and $u_{\max}(x)$ can be used instead.

3.2.2 Calculating δ_i

To mathematically define the inertial boundary thickness $\delta_i(x)$ we cast the velocity profile into a probability density function moment framework. To do this we define velocity profiles central moments of $(u(y)/u_\infty)-1$ as

$$\gamma_n = \int_{\delta_{\max}}^{h} dy \left(y-\kappa\right)^n \frac{1}{\delta_1^i}\left\{\frac{u(y)}{u_\infty}-1\right\} \quad , \tag{4}$$

where $y = h$ is deep into the free stream, where the mean location κ is given by

$$\kappa = \int_{\delta_{\max}}^{h} dy\, y \frac{1}{\delta_1^i} \left\{ \frac{u(y)}{u_\infty} - 1 \right\} \quad , \tag{5}$$

and where the modified inertial displacement thickness is

$$\delta_1^i = \int_{\delta_{\max}}^{h} dy \left\{ \frac{u(y)}{u_\infty} - 1 \right\} \quad . \tag{6}$$

At this point we can go ahead and construct the various thickness and shape parameters in terms of the mean location and higher order moments of γ_n as was demonstrated by Weyburne.[3] The four-sigma $\delta_i(x) = \kappa + 4\sqrt{\gamma_2}$ value, for example, corresponds to the point where $u(x, y)$ essentially becomes the free stream velocity u_∞. It is important to point out that we could have made the above definitions with $\delta_v(x)$ in place of $\delta_{\max}(x)$. We opted for the $\delta_{\max}(x)$ based definition since $\delta_v(x)$ is only easily calculated for computer simulation data where the second derivative data is readily available and free of experimental measurement noise.

4. THE INERTIAL BOUNDARY LAYER MOMENTUM EQUATIONS

In this Section, we examine the possibility for finding a simple theoretical representation for the velocity and pressure fields for the inertial boundary layer. The velocity and pressure fields in this region have been obtained by solving the inviscid flow governing equations using computer-based packages of which a number are available. However, these computer-based numerical solutions cannot be used to develop a theoretical treatment of lift/drag. One viable theoretical path is to seek similarity solutions for the inertial boundary layer and combine those solutions with the Blasius[5] and Falkner-Skan[6] solutions for the viscous boundary layer region to make a theoretical treatment for lift/drag on an airfoil. This approach will only work if the **scaled** velocity profiles are truly similar. This can never happen for $u(x,y)$ profiles since at one extreme $u(x,\delta_{\max})=u_{\max}(x)$ is a function of *x* but the other extreme $u(x,y)$ becomes u_∞ which does not change with *x* and is nonzero. Therefore, a simple scaling parameter that is a function of *x* cannot result in similar profiles. However, for the flat plate case, $u_{\max}(x)$ is almost constant so similar-like profiles are possible. Rather than seeking solutions for $u(x,y)$, we introduce the velocity $w(x,y)$ defined as

$$w(x,y) \;=\; u(x,y)-u_\infty \quad . \tag{7}$$

We can substitute $w(x,y)+u_\infty$ for $u(x,y)$ into the flow governing equations which then becomes a set of differential equations for $w(x,y)$ and $v(x,y)$. The advantage of using $w(x,y)$ is that $w(x,y)$ is the same order of magnitude as $v(x,y)$ making the numerical solution process straightforward.

The process of finding similar solutions begins by putting the flow governing equations into dimensionless form. The first step in this process is to introduce length and velocity scaling parameters. At this point in time, there is no theoretical indication as to what the correct scaling parameter should be. Weyburne[7] used an integral area treatment to prove that the displacement thickness $\delta_s(x)$ and the velocity at the boundary layer edge $u_e(x)$ must be similarity scaling parameters for wind tunnel type flow. A similar proof may be possible for the unbounded flow case also but until then we will retain the generic unknown scaling parameter $u_s(x)$ as the velocity scaling parameter. The velocity scaling parameter $u_s(x)$ must make plots of $w(x,y)$ along the airfoil appear similar. In the same way, we assume a generic length scaling parameter $\delta_s(x)$, so that the scaled *y*-variable is given by

$$\eta \;=\; \frac{y}{\delta_s(x)} \quad . \tag{8}$$

Although we have no theoretical guidance, we can make some intelligent guesses as to the identities of the scaling parameters $\delta_s(x)$ and $u_s(x)$ that hopefully will collapse a set of velocity profiles in the inertial boundary layer region to single curve. If we can do that, then we can reduce the PDE governing equations to simple ODEs. In Section 5 below, we show that the velocity at

the viscous boundary layer edge $u_e(x) \cong u_{\max}(x)$ is a good velocity scale for the viscous region that borders the inertial region. The two regions border each other at the point where $u(x,y) = u_{\max}(x)$. It therefore makes sense that same scaling should also work in the inertial region. Hence, we will assume $u_s(x)$ in the inertial boundary layer region also scales as $u_{\max}(x)$. That is,

$$u_s(x) = u_{\max}(x) \cong u(x, \delta_v^{2.6}) \quad . \tag{9}$$

Although we do not have any theoretical direction for choosing the identity for $\delta_s(x)$, it is by definition that the inertial displacement thickness δ_1^i (Eq. 6) will normalize the area under all of the scaled $w(x,y)/u_{\max}(x)$ profiles. Weyburne[7] proved that the displacement thickness must be a similar scaling parameter for the 2D wind tunnel-based boundary layer. Therefore, as a first guess, we assume that the length scaling parameter goes as the displacement thickness δ_1^i. In Figs. 7a and 7b, we show a plot of a range of $w(x,y)/u_{\max}(x)$ profiles versus *y*/*c* and y/δ_1^i. The collapse of the curves in Fig. 7b is not exact but similar-like. The collapse is close enough to expect good results if we go ahead and assume that similar behavior exists in this region.

The success of Fig. 7b gives us some reasonable expectation that the flow in the inertial boundary layer region can be modeled using a similarity solution. The similarity solution for the inertial boundary layer proceeds by introducing scaling parameters that reduce the set of flow governing partial differential equations (PDEs) to a set of ordinary differential equations (ODEs). Given that most of the same conditions apply in the inertial region as the viscous boundary layer region, we can assume that the Prandtl boundary layer equation approximations apply in this region. In Appendix A, B, and C we detail the process of nondimensionalizing the resulting flow governing equations for the inertial boundary layer region.

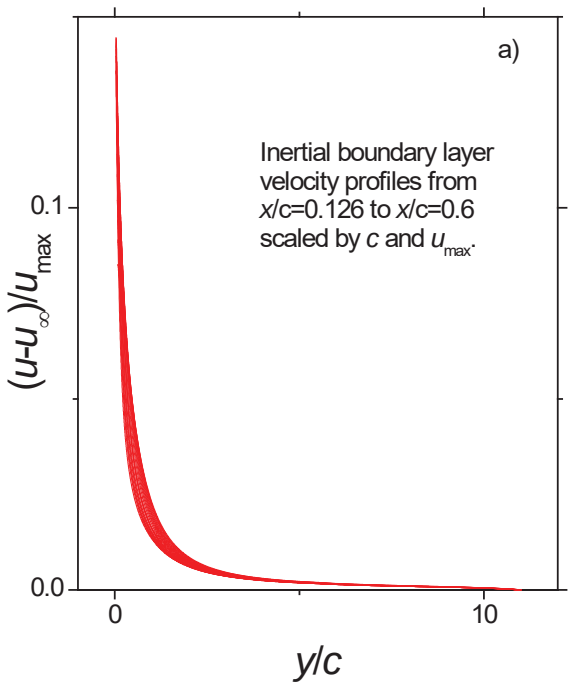

Figure 7a: Inertial Boundary Layer Velocity Profiles from Swanson and Langer[4]

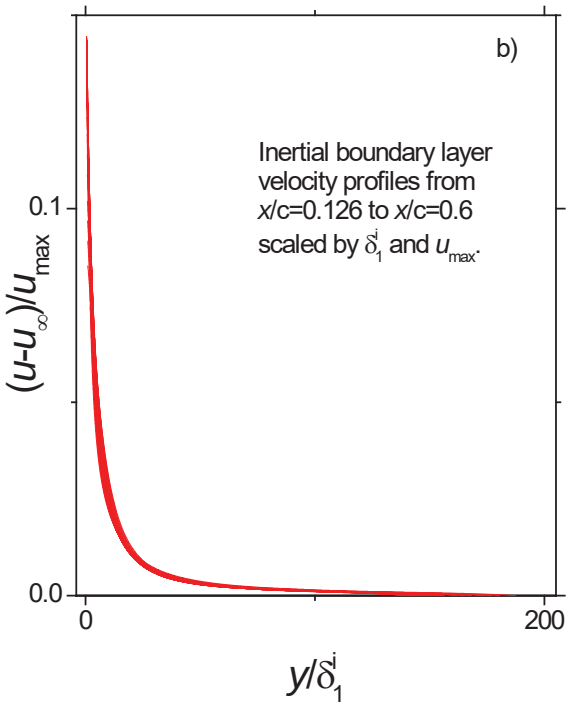

Figure 7b: Same as Figure 7a but *y*-scaling changed to δ_1^i Scaling

5. THE VISCOUS BOUNDARY LAYER

The section above indicates that similar solutions may work for the inertial boundary layer region. This means that it may be possible to put together a complete theoretical treatment for lift-drag on an airfoil. What we propose is to combine the similar solutions for the inertial region along with the similar solutions for the viscous region. An energy minimization scheme would be used to discover the unknown parameters involved in the similar solutions. Part of that scheme relies on the assumption that the near wall viscous region is amendable to theoretical treatment. In fact, the success of the panel solution methods, such as Drela and Gile's[8] Xfoil, in terms of predicting lift and drag profiles for various airfoils is proof that a simple characterization of the viscous boundary layer using Blasius[5] and Falkner-Skan[6] integral solutions may be adequate. However, to our knowledge, there has been no direct experimental confirmation showing a comparison of experimental airfoil data in the viscous region to the theoretical treatments.

For confirmation, we examined the APG and ZPG regions of the NACA0012 simulation data from Swanson and Langer.[4] For the airfoil at zero degrees, most of the airfoils surface consist of ZPG and APG regions. From examination of the simulation data, we will assume that the ZPG region extends from about x/c=0.12 to x/c=0.3 and the APG region from x/c=0.3 to x/c=0.6. In Fig. 8 we show plots of the scaled velocity profiles compared to the similarly scaled Blasius profile for the ZPG region. The scaled velocity profile plots show good overlap with the Blasius profile. In Fig. 9 we show the set of scaled profiles constituting the approximate APG region. The scaled velocity profiles show good overlap with the scaled Falkner-Skan profile. This overlap was accomplished by examining the plot of the scaled profiles show in Fig. 9, and then adjusting power law power exponent m in the Falkner-Skan solution until we obtained a good overlap. For the APG region, we found m=-0.07 works reasonably well.

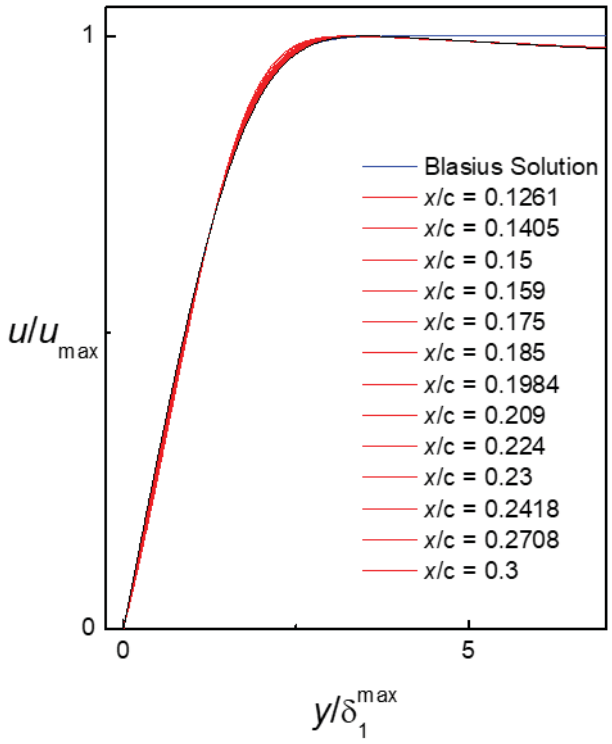

Figure 8: ZPG Viscous Region Velocity Profiles from Swanson and Langer[4]

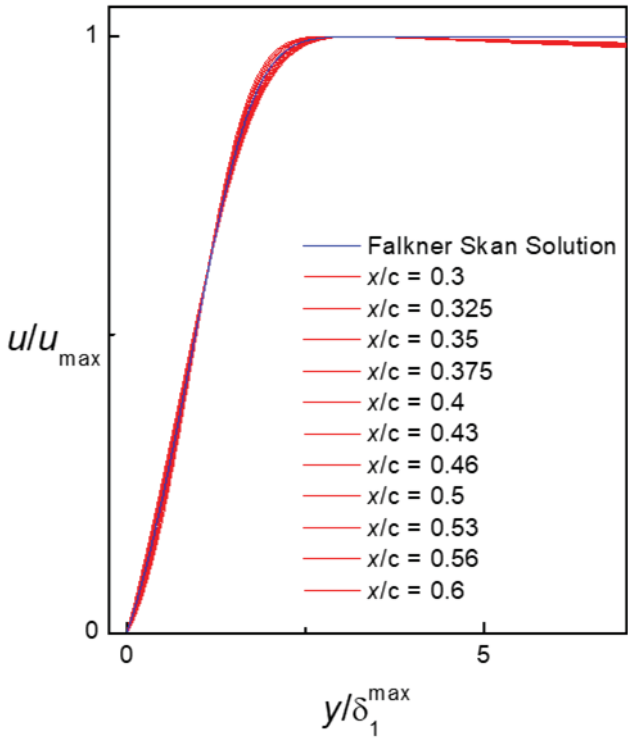

Figure 9: APG Viscous Region Velocity Profiles from Swanson and Langer[4] with m=-0.07

6. DISCUSSION

The traditional boundary layer model is obviously inadequate to fully describe unbounded flow along a wall. The traditional boundary layer model assumes that the velocity profile at a position *x* along the wall asymptotes to a constant value $u_e(x)$ whose value that may change as one moves along the wall. This model appears to be partly driven by the theoretical approaches of Blasius[5] and Falkner-Skan[6] (they assume an asymptotic velocity) and partly by wind tunnel measurements. Most wind tunnel experiments do in fact show this asymptotic behavior. However, it is also obvious that this asymptotic behavior in the wind tunnel is not what one would expect for a boundary layer on a plate in an unbounded moving fluid mass. In the wind tunnel, the asymptotic behavior is created by the interaction of the plate's boundary layer and the hydrodynamically close top and bottom walls. This type of flow is what one expects in 2-D closed channel flow with a large gap separation. An unbounded moving fluid impacting on a wall-plate-airfoil, on the other hand, asymptotes to the inlet free stream velocity u_∞. To address this issue for the unbounded flow situation, we added an additional inertial boundary layer region to the traditional viscous boundary layer description. The inertial boundary layer description is depicted in Fig. 2 for our new boundary layer concept.

It is worth commenting on the traditional boundary layer model in that it brings up a disturbing reality of the wind tunnel datasets obtained to date. If the top wall is interacting with the boundary layer along the plate then what do we know about the boundary layer along the top wall? The answer for many wind tunnel datasets is very little. From what I have observed, the top and bottom wall effects in a wind tunnel are rarely discussed. To a certain extent, this is acceptable for some purposes but it easy to imagine how the top wall could have unintended effects on the main boundary layer measurements. For example, the laminar-turbulent transition point on the main measurement plate-airfoil could obviously be influenced by the presence of the laminar-turbulent transition on the top wall which could occur at a different wall location due to a different wall roughness, for example. It is also probably true that the gap distance could have unintended effects on the measured flow. Is there a difference in the flow when the gap distance is just enough to affect the main measurement plate-airfoil boundary layer versus flow where the gap is much smaller? What about the effect of turbulence on the gap distance? Are the turbulent statistics affected by the gap distance? Unfortunately, the answer to these questions are often unknown or unreported. This puts a cloud of uncertainty in making comparison of different wind tunnel results in certain situations.

Although not the original intent of this report, we found that the new inertial region could be the key to a problem that has persisted for more than 100 years, and that is that there has yet to be a good theoretical explanation of airfoil lift. The panel methods like the Xfoil package of Drela and Giles[8] are a step in that direction but the fact that the inertial regions are handled by numerical methods means the approach is only partially theoretical. Since we showed that the inertial region discussed above can be approximated theoretically by similar solutions, then this means that a complete theoretical approach may be possible. With this addition, we now have the basis for a possible bare bones theory of lift and drag. For the viscous near wall region, standard Falkner-Skan theory may be adequate as demonstrated by Xfoil-type lift-drag prediction successes and by Figs. 8 and 9. For the inertial region, the new similarity formulation appears to be adequate as indicated by Fig. 7. To tie the two regions together, we need to

consider the boundary between the viscous and inertial regions. At the boundary, we note that the viscous boundary layer Falkner-Skan solutions provide the necessary boundary condition information for the inertial boundary layer solution. In particular, it provides the *x*-pressure gradient boundary value and *y*-pressure[9] gradient boundary values at the boundary between the two regions as well as the values for the constants of the similarity scaling parameters (Eqs. A10 and A12). Matching the scaled pressure gradients boundary conditions at the viscous-inertial boundary is one of the keys to a path to a complete theory for flow over an airfoil. The other set of unknowns is the location of the different pressure gradient zone boundaries. What we propose is that one way of doing this is to borrow from the panel method idea and seek energy minima to establish pressure gradient boundaries.

7. CONCLUSION

A new boundary layer model for describing the laminar flow along a wall in an unbounded moving airmass is introduced. The model consists of a viscous boundary layer region and an inertial boundary layer region. The inertial region above the viscous boundary layer is found to be well represented by similar-like velocity profiles. A set of ODEs for the pressure gradients are obtained. It is pointed out that by stitching together the viscous and inertial boundary layer regions may make it possible to theoretically describe the velocity and pressure fields along an airfoil and provide a complete theoretical treatment of airfoil lift and drag.

Acknowledgement

The author thanks the authors Stefan Langer and Ronald Swanson for making their dataset available for use in this report. The author also acknowledges the support of the Air Force Research Laboratory and Gernot Pomrenke at the Air Force Office of Scientific Research.

8. REFERENCES

[1]L. Prandtl, "Über Flüssigkeitsbewegung bei sehr kleiner Reibung," Verhandlungen des Dritten Internationalen Mathematiker-Kongresses in Heidelberg 1904.

[2]D. Weyburne, "A mathematical description of the fluid boundary layer, " Applied Mathematics and Computation," **175**, 1675 (2006). Also D. Weyburne, Erratum, Applied Mathematics and Computation, **197**, 466 (2008).

[3]D. Weyburne, "New thickness and shape parameters for the boundary layer velocity profile," Experimental Thermal and Fluid Science, **54**, 22(2014).

[4]R. Swanson and S. Langer, "Comparison of NACA 0012 Laminar Flow Solutions: Structured and Unstructured Grid Methods," NASA/TM-2016-219003.

[5]H. Blasius, "Grenzschichten in Flüssigkeiten mit kleiner Reibung," Zeitschrift für Mathematik und Physik, **56**, 1(1908).

[6]V. Falkner and S. Skan, Aero. Res. Coun. Rep. and Mem. no 1314, 1930.

[7]D. Weyburne, "Similarity of the Velocity Profile," Air Force Tech report AFRL-RY-WP-TR-2014-0227, https://discover.dtic.mil/, ADA609962, 2014.

[8]M. Drela and M. Giles, "Viscous-Inviscid Analysis of Transonic and Low Reynolds Number Airfoils," AIAA J., **25**, 1347(1989).

[9]D. Weyburne, "The normal to the wall pressure gradients for Blasius and Falkner-Skan boundary layer flow," Air Force Tech report AFRL-RY-WP-TR-2018-0153, https://discover.dtic.mil/, 2018.

APPENDIX A: THE INERTIAL BOUDARY LAYER MOMENTUM EQUATION

For the inertial boundary layer region, conservation of momentum, energy, and mass governs the behavior of the fluid flow. We assume that the same boundary layer equations proposed by Ludwig Prandtl[1] also applies for this case since most of the same conditions that led to the Prandtl boundary layer conservation equations apply to the inertial region as well. Thus, for an isothermal 2-D incompressible laminar flow, we assume that the x-component of the momentum balance (parallel to the wall) is given by

$$u(x,y)\frac{\partial u(x.y)}{\partial x} + v(x,y)\frac{\partial u(x,y)}{\partial y} = -\frac{1}{\rho}\frac{\partial P}{\partial x} + \nu\frac{\partial^2 u(x,y)}{\partial y^2} \quad , \tag{A1}$$

where ρ is the density, ν is the kinematic viscosity, P is the pressure, $u(x,y)$ is the velocity in the x-direction, and $v(x,y)$ is the velocity in the y-direction. We also assume the y-component of the momentum balance (normal to the wall) is given by

$$u(x,y)\frac{\partial v(x,y)}{\partial x} + v(x,y)\frac{\partial v(x,y)}{\partial y} = -\frac{1}{\rho}\frac{\partial P}{\partial y} + \nu\frac{\partial^2 v(x,y)}{\partial y^2} \quad , \tag{A2}$$

and the mass conservation equation is given by

$$\frac{\partial u(x,y)}{\partial x} + \frac{\partial v(x,y)}{\partial y} = 0 \quad . \tag{A3}$$

In order to reduce these PDE equations to a set of ODE, we start by introducing a stream function. We assume that a stream function $\psi(x,y)$ exists such that

$$\frac{\psi(x,y)}{\delta_s(x)u_s(x)} = g(\eta) \quad , \tag{A4}$$

where $g(\eta)$ is a dimensionless function that only depends on the scaled y-position η (given by Eq. 8), and that the stream function satisfies the conditions

$$u(x,y) = \frac{\partial\psi(x,y)}{\partial y}, \qquad v(x,y) = -\frac{\partial\psi(x,y)}{\partial x} \quad . \tag{A5}$$

The velocity $v(x,y)$ can be expressed as

$$\begin{aligned} v(x,y) &= -\frac{\partial \psi}{\partial x} = -\frac{\partial}{\partial x}\{\delta_s u_s g(\eta)\} = -\frac{d\{\delta_s u_s\}}{dx} g - \delta_s u_s \frac{\partial g}{\partial x} \\ v(x,y) &= -(u_s \delta_s' + u_s' \delta_s) g - \delta_s u_s \left(\frac{\partial g}{\partial \eta} \frac{\partial \eta}{\partial x} \right) \\ v(x,y) &= -(u_s \delta_s' + u_s' \delta_s) g - \delta_s u_s \left(-\frac{\eta \delta_s'}{\delta_s} g' \right) \\ v(x,y) &= -(u_s \delta_s' + u_s' \delta_s) g + \delta_s' u_s \eta g' \quad , \end{aligned} \tag{A6}$$

where the prime indicates differentiation with respect to η for functions of η and the prime indicates differentiation with respect to x for functions of x. Eq. A6 uses the fact that

$$\frac{\partial \eta}{\partial x} = \frac{\partial}{\partial x}\left\{ \frac{y}{\delta_s(x)} \right\} = y \frac{d\{1/\delta_s\}}{dx} = -y \frac{\delta_s'}{\delta_s^2} = -\frac{\eta \delta_s'}{\delta_s} \tag{A7}$$

The velocity $w(x,y)$, where $w(x,y) = u(x,y) - u_\infty$, becomes

$$\begin{aligned} w(x,y) + u_\infty &= u(x,y) = \frac{\partial \psi}{\partial y} = \frac{\partial\{\delta_s u_s g(\eta)\}}{\partial y} \\ w(x,y) + u_\infty &= \delta_s u_s \frac{\partial g}{\partial y} = \delta_s u_s \frac{\partial g}{\partial \eta} \frac{\partial \eta}{\partial y} = \delta_s u_s g' \frac{1}{\delta_s} \\ w(x,y) + u_\infty &= u_s g' \quad , \end{aligned} \tag{A8}$$

where we have used the fact that

$$\frac{\partial \eta}{\partial y} = \frac{\partial}{\partial y}\left\{ \frac{y}{\delta_s(x)} \right\} = \frac{1}{\delta_s} \quad . \tag{A9}$$

The velocities given by given by Eqs. A6 and A8 can now be substituted into the momentum equations (Eqs. A1 and A2). The term by term transformation is delineated in Appendix B and C. The important result obtained from the transformed x-component of the momentum balance (Eq. A1) is that

$$-\frac{1}{\rho(u_s u_s' + u_s^2 \delta_s' / \delta_s)} \frac{\partial P}{\partial x} = g g'' + \alpha_1 g'^2 - \alpha_2 g''' \quad , \tag{A10}$$

where

$$\alpha_1 = \frac{u_s u_s'}{u_s^2 \delta_s' / \delta_s + u_s u_s'} \quad \text{and} \quad \alpha_2 = \frac{\nu u_s}{\delta_s^2 (u_s^2 \delta_s' / \delta_s + u_s u_s')} \quad . \tag{A11}$$

In a similar fashion (see Appendix C), the transformed *y*-momentum equation (Eq. A2) reduces to

$$-\frac{1}{\rho(u_s u_s' \delta_s' + u_s^2 \delta_s'')} \frac{\partial P}{\partial y} = -\beta_1 g g' + \eta g'^2 - \beta_2 \eta g g'' + \beta_3 g'' - \beta_4 \eta g''' \quad , \tag{A12}$$

where

$$\beta_1 = \frac{u_s^2 \delta_s'' + u_s'' u_s \delta_s + u_s' u_s \delta_s' - u_s'^2 \delta_s}{u_s u_s' \delta_s' + u_s^2 \delta_s''} \quad \text{and} \quad \beta_2 = \frac{\frac{u_s^2 \delta_s'^2}{\delta_s} + u_s u_s' \delta_s'}{u_s u_s' \delta_s' + u_s^2 \delta_s''} \quad , \tag{A13}$$

and where

$$\beta_3 = \nu \frac{\frac{u_s \delta_s'}{\delta_s^2} - \frac{u_s'}{\delta_s}}{u_s u_s' \delta_s' + u_s^2 \delta_s''} \quad \text{and} \quad \beta_4 = \nu \frac{\frac{u_s \delta_s'}{\delta_s^2}}{u_s u_s' \delta_s' + u_s^2 \delta_s''} \quad . \tag{A14}$$

Similarity requires α_1, α_2, β_1, β_2, β_3, and β_4, must be constant (no x-dependence).

The results shown in Fig. 7 indicate that the velocity at the viscous boundary layer edge $u_e(x) \cong u_{\max}(x)$ is a good velocity scale for the viscous region. We can take this a step further since we know from the Blasius and Falkner-Skan solutions for the viscous boundary layer that the velocity at the viscous boundary layer edge $u_e(x)$ must be a simple power function of the distance along the plate. Thus, we assume that the scaling in the inertial boundary layer region must also be given by

$$u_s(x) = u_e(x) = a_i (x - x_0)^{m_i} \quad , \tag{A15}$$

where a_i, x_0, and m_i are constants.

Having assumed that the velocity scaling parameter goes as a simple power function of *x*, we go ahead and assume that the length scaling parameter δ_s is also be a power function of *x* so that

$$\delta_s(x) \;=\; \delta_1^i(x) \;=\; b_i(x-x_0)^{n_i} \quad , \tag{A16}$$

where b_i, x_0, and n_i are constants.

With these assumptions, the pressure gradients, Eqs. A10 and A12, should reduce to the something close to the well-known Falkner-Skan equations. The difference is that we make no assumptions at this point for the behavior of the pressure gradient $\partial P/\partial x$ itself. If we substitute Eqs. A15 and A16 into Eqs. A11, A13, and A14, then

$$\alpha_1 \;=\; \frac{m_i}{m_i+n_i} \quad \text{and} \quad \alpha_2 \;=\; \frac{\nu}{a_i b_i^2 (m_i+n_i)}(x-x_0)^{-m_i-2n_i+1} \quad , \tag{A17}$$

and

$$\beta_1 \;=\; \frac{(m+n)(n-1)}{n(m+n-1)} \quad \text{and} \quad \beta_2 \;=\; \frac{m+n}{m+n-1} \quad , \tag{A18}$$

and where

$$\beta_3 \;=\; \frac{\nu}{a_i b_i^2}\frac{(n_i-m_i)(x-x_0)^{-m_i-2n_i+1}}{n_i(m_i+n_i-1)} \quad \text{and} \quad \beta_4 \;=\; \frac{\nu}{a_i b_i^2}\frac{(x-x_0)^{-m_i-2n_i+1}}{n_i(m_i+n_i-1)} \quad . \tag{A19}$$

Notice that α_1, α_2, β_1, β_2, β_3, and β_4 must be constants (no direct *x*-dependence) which means that $m_i + 2n_i - 1 = 0$. However, this condition only holds if the viscous terms in the inertial region are important. If the solutions indicate the viscous terms are negligible, then the condition that $m_i + 2n_i - 1 = 0$ is no longer applicable and the constants α_2, β_3, and β_4 are eliminated.

APPENDIX B: *X*-COMPONENT OF THE INERTIAL MOMENTUM EQUATION

In this Section, we will delineate the steps to obtain the nondimensionalized *x*-component of the momentum equation by substituting the reduced velocities given by Eqs. A6 and A8 into the Prandtl *x*-component of the momentum equation (Eq. A1); starting on the left-hand side, we have

$$\begin{aligned}(w+u_\infty)\frac{\partial(w+u_\infty)}{\partial x} &= u_s g'\frac{\partial\{u_s g'\}}{\partial x} = u_s g'\left(\frac{du_s}{dx}g' + u_s\frac{\partial g'}{\partial\eta}\frac{\partial\eta}{\partial x}\right)\\ &= u_s g'\left(u_s' g' - u_s\frac{\eta\delta_s'}{\delta_s}g''\right)\\ &= u_s u_s' g'^2 - \frac{u_s^2\delta_s'}{\delta_s}\eta g' g'' \quad .\end{aligned} \tag{B1}$$

The next term in Eq. A1 we need to nondimensionalize is

$$\begin{aligned}v\frac{\partial\{w+u_\infty\}}{\partial y} &= \left\{-(u_s\delta_s' + u_s'\delta_s)g + \delta_s' u_s\eta g'\right\}u_s\frac{\partial g'}{\partial\eta}\frac{\partial\eta}{\partial y}\\ &= \left\{-(u_s\delta_s' + u_s'\delta_s)g + \delta_s' u_s\eta g'\right\}u_s g''\frac{1}{\delta_s}\\ &= \left\{-(u_s\delta_s' + u_s'\delta_s)g + \delta_s' u_s\eta g'\right\}\frac{u_s}{\delta_s}g''\\ &= -\frac{u_s^2\delta_s'}{\delta_s}gg'' - u_s u_s' gg'' + \frac{u_s^2\delta_s'}{\delta_s}\eta g' g'' \quad .\end{aligned} \tag{B2}$$

Combining the first two transformed terms, we have

$$\begin{aligned}\{w+u_\infty\}\frac{\partial\{w+u_\infty\}}{\partial x} + v\frac{\partial\{w+u_\infty\}}{\partial y} &= u_s u_s' g'^2 - \frac{u_s^2\delta_s'}{\delta_s}\eta g' g'' - \frac{u_s^2\delta_s'}{\delta_s}gg'' +\\ &\qquad - u_s u_s' gg'' + \frac{u_s^2\delta_s'}{\delta_s}\eta g' g''\end{aligned} \tag{B3}$$

$$\{w+u_\infty\}\frac{\partial\{w+u_\infty\}}{\partial x} + v\frac{\partial\{w+u_\infty\}}{\partial y} = u_s u_s' g'^2 - \frac{u_s^2\delta_s'}{\delta_s}gg'' - u_s u_s' gg'' \quad .$$

Until we know otherwise, we will retain the viscous terms (see Discussion). The viscous term is given by

$$\begin{aligned} \nu\frac{\partial^2 u(x,y)}{\partial y^2} &= \nu\frac{\partial^2\{w+u_\infty\}}{\partial y^2} = \nu u_s\frac{\partial}{\partial y}\left\{\frac{\partial g'}{\partial\eta}\frac{\partial\eta}{\partial y}\right\} \\ \nu\frac{\partial^2 u(x,y)}{\partial y^2} &= \nu u_s\frac{\partial}{\partial\eta}\left\{g''\frac{1}{\delta_s}\right\}\frac{\partial\eta}{\partial y} \\ \nu\frac{\partial^2 u(x,y)}{\partial y^2} &= \nu\frac{u_s}{\delta_s^2}g''' \quad . \end{aligned} \tag{B4}$$

This means the reduced Prandtl *x*-component of the inertial momentum balance is given by

$$\begin{aligned} u_s u_s' g'^2 - \frac{u_s^2\delta_s'}{\delta_s}gg'' - u_s u_s' gg'' &= -\frac{1}{\rho}\frac{\partial P}{\partial x} + \nu\frac{u_s}{\delta_s^2}g''' \\ -\frac{1}{\rho}\frac{\partial P}{\partial x} &= \left(\frac{u_s^2\delta_s'}{\delta_s} + u_s u_s'\right)gg'' + u_s u_s' g'^2 - \nu\frac{u_s}{\delta_s^2}g''' \quad . \end{aligned} \tag{B5}$$

For velocity profile similarity, we must have the *x*-dependent portion of each term change in the same way as we move along the plate. Equivalently, if we divide through by one of the *x*-terms then the resulting *x*-dependent ratios must be constant. Dividing Eq. A13 through by $u_s u_s' + u_s^2\delta_s'/\delta_s$, we end up the transformed x-component of the momentum balance (Eq. A1) as

$$-\frac{1}{\rho(u_s u_s' + u_s^2\delta_s'/\delta_s)}\frac{\partial P}{\partial x} = gg'' + \alpha_1 g'^2 - \alpha_2 g''' \quad , \tag{B6}$$

where

$$\alpha_1 = \frac{u_s u_s'}{u_s^2\delta_s'/\delta_s + u_s u_s'} \quad \text{and} \quad \alpha_2 = \frac{\nu u_s}{\delta_S^2(u_s^2\delta_s'/\delta_s + u_s u_s')} \quad . \tag{B7}$$

APPENDIX C: *Y*-COMPONENT OF THE INERTIAL MOMENTUM EQUATION

The reduced *y*-component of the Prandtl momentum equations is generated in a similar fashion. Substituting the reduced velocities given by Eqs. A6 and A8 into the Prandtl *y*-component of the momentum equation (Eq. A2); starting on the left-hand side, we have

$$
\begin{aligned}
(w+u_\infty)\frac{\partial v}{\partial x} &= u\frac{\partial v}{\partial x} = u_s g'\frac{\partial\left\{-(u_s\delta_s' + u_s'\delta_s)g + \delta_s' u_s \eta g'\right\}}{\partial x} \\
&= u_s g'\left\{\begin{array}{l} -(u_s'\delta_s' + u_s\delta_s'' + u_s''\delta_s + u_s'\delta_s')g - (u_s\delta_s' + u_s'\delta_s)\dfrac{\partial g}{\partial x} \\ +(\delta_s'' u_s + \delta_s' u_s')\eta g' + \delta_s' u_s \dfrac{\partial \eta g'}{\partial \eta}\dfrac{\partial \eta}{\partial x} \end{array}\right\} \qquad \text{(C1)} \\
&= u_s g'\left\{\begin{array}{l} -(2u_s'\delta_s' + u_s\delta_s'' + u_s''\delta_s)g - (u_s\delta_s' + u_s'\delta_s)g'\left\{-\dfrac{\eta\delta_s'}{\delta_s}\right\} \\ +(\delta_s'' u_s + \delta_s' u_s')\eta g' + \delta_s' u_s (g' + \eta g'')\left\{-\dfrac{\eta\delta_s'}{\delta_s}\right\} \end{array}\right\} \\
&= u_s g'\left\{\begin{array}{l} -(2u_s'\delta_s' + u_s\delta_s'' + u_s''\delta_s)g + (\dfrac{u_s\delta_s'^2}{\delta_s} + u_s'\delta_s')\eta g' \\ +(\delta_s'' u_s + \delta_s' u_s')\eta g' - \dfrac{\delta_s'^2 u_s}{\delta_s}(\eta g' + \eta^2 g'') \end{array}\right\} \\
&= -(2u_s u_s'\delta_s' + u_s^2\delta_s'' + u_s'' u_s\delta_s)gg' + (\frac{u_s^2\delta_s'^2}{\delta_s} + 2u_s u_s'\delta_s' + u_s^2\delta_s'')\eta g'^2 + \\
&\quad -\frac{u_s^2\delta_s'^2}{\delta_s}(\eta g'^2 + \eta^2 f' g'') \\
&= -(2u_s u_s'\delta_s' + u_s^2\delta_s'' + u_s'' u_s\delta_s)gg' + (2u_s u_s'\delta_s' + u_s^2\delta_s'')\eta g'^2 + \\
&\quad -\frac{u_s^2\delta_s'^2}{\delta_s}\eta^2 g' g'' \quad .
\end{aligned}
$$

The next term is

$$
\begin{aligned}
\nu\frac{\partial v}{\partial y} &= \nu\frac{\partial\left\{-(u_s\delta_s{}' + u_s{}'\delta_s)g + \delta_s{}' u_s\eta g'\right\}}{\partial y} \\
&= \nu\left\{-(u_s\delta_s{}' + u_s{}'\delta_s)\frac{\partial g}{\partial\eta}\frac{\partial\eta}{\partial y} + \delta_s{}' u_s\frac{\partial\eta g'}{\partial\eta}\frac{\partial\eta}{\partial y}\right\} \\
&= \nu\left\{-(u_s\delta_s{}' + u_s{}'\delta_s)\,g'\frac{1}{\delta_s} + \delta_s{}' u_s\left\{g' + \eta g''\right\}\frac{1}{\delta_s}\right\} \\
&= \left\{-(u_s\delta_s{}' + u_s{}'\delta_s)g + \delta_s{}' u_s\eta g'\right\}\left\{-(\frac{u_s\delta_s{}'}{\delta_s} + u_s{}')g' + \frac{\delta_s{}' u_s}{\delta_s}\left\{g' + \eta g''\right\}\right\} \\
&= (\frac{u_s^2\delta_s{}'^2}{\delta_s} + u_s u_s{}'\delta_s' + u_s u_s{}'\delta_s' + u_s{}'^2\delta_s)gg' - (\frac{u_s^2\delta_s{}'^2}{\delta_s} + \delta_s' u_s u_s{}')\eta g'^2 \\
&\quad -(\frac{u_s^2\delta_s{}'^2}{\delta_s} + u_s u_s{}'\delta_s')\left\{gg' + \eta gg''\right\} + \frac{u_s^2\delta_s{}'^2}{\delta_s}\left\{\eta g'^2 + \eta^2 g'g''\right\} \\
&= (u_s u_s{}'\delta_s' + u_s{}'^2\delta_s)gg' \; - (\frac{u_s^2\delta_s{}'^2}{\delta_s} + u_s u_s{}'\delta_s')\eta gg'' \\
&\quad - \delta_s' u_s u_s{}'\eta g'^2 + \frac{u_s^2\delta_s{}'^2}{\delta_s}\eta^2 g'g'' \quad .
\end{aligned}
\tag{C2}
$$

For the purpose of finding the local energy minimum in our eventual lift/drag theory, we will retain the viscous terms (see Discussion). The viscous term is given by

$$
\begin{aligned}
\nu\frac{\partial^2 v(x,y)}{\partial y^2} &= \nu\frac{\partial}{\partial y}\left\{\frac{\partial\left\{-(u_s\delta_s{}' + u_s{}'\delta_s)g + \delta_s{}' u_s\eta g'\right\}}{\partial y}\right\} \\
\nu\frac{\partial^2 v(x,y)}{\partial y^2} &= \nu\frac{\partial}{\partial\eta}\left\{-(u_s\delta_s{}' + u_s{}'\delta_s)\frac{\partial g}{\partial\eta}\frac{\partial\eta}{\partial y} + \delta_s{}' u_s\frac{\partial\eta g'}{\partial\eta}\frac{\partial\eta}{\partial y}\right\}\frac{\partial\eta}{\partial y} \\
&= \nu\frac{\partial}{\partial\eta}\left\{-(u_s\delta_s{}' + u_s{}'\delta_s)\,g'\frac{1}{\delta_s} + \delta_s{}' u_s\left\{g' + \eta g''\right\}\frac{1}{\delta_s}\right\}\frac{1}{\delta_s} \\
&= -\nu(\frac{u_s\delta_s{}'}{\delta_s^2} + \frac{u_s{}'}{\delta_s})\,g'' + \nu\frac{u_s\delta_s{}'}{\delta_s^2}\left\{g'' + g'' + \eta g'''\right\} \\
&= \nu(\frac{u_s\delta_s{}'}{\delta_s^2} - \frac{u_s{}'}{\delta_s})\,g'' + \nu\frac{u_s\delta_s{}'}{\delta_s^2}\eta g''' \qquad .
\end{aligned}
\tag{C3}
$$

Combining all of the terms, we have

$$
\begin{aligned}
&-(\cancel{u_s u_s' \delta_s'} + u_s^2 \delta_s'' + u_s'' u_s \delta_s + u_s' u_s \delta_s')gg' + (\cancel{2} u_s u_s' \delta_s' + u_s^2 \delta_s'')\eta g'^2 + \\
&\cancel{-\frac{u_s^2 \delta_s'^2}{\delta_s} \eta^2 g' g''} \quad + \\
&+(\cancel{u_s u_s' \delta_s'} + u_s'^2 \delta_s)gg' - (\frac{u_s^2 \delta_s'^2}{\delta_s} + u_s u_s' \delta_s')\eta g g'' \\
&\cancel{-\delta_s' u_s u_s' \eta g'^2} + \cancel{\frac{u_s^2 \delta_s'^2}{\delta_s} \eta^2 g' g''} \\
&= -(u_s^2 \delta_s'' + u_s'' u_s \delta_s + u_s' u_s \delta_s' - u_s'^2 \delta_s)gg' + (u_s u_s' \delta_s' + u_s^2 \delta_s'')\eta g'^2 \\
&\quad -(\frac{u_s^2 \delta_s'^2}{\delta_s} + u_s u_s' \delta_s')\eta g g'' \\
&= \quad -\frac{1}{\rho}\frac{\partial P}{\partial y} - \nu(\frac{u_s \delta_s'}{\delta_s^2} - \frac{u_s'}{\delta_s})g'' + \nu \frac{u_s \delta_s'}{\delta_s^2}\eta g''' \qquad .
\end{aligned}
\tag{C4}
$$

Dividing through by $u_s u_s' \delta_s' + u_s^2 \delta_s''$, the y-momentum equation becomes

$$
-\frac{1}{\rho(u_s u_s' \delta_s' + u_s^2 \delta_s'')}\frac{\partial P}{\partial y} = -\beta_1 gg' + \eta g'^2 - \beta_2 \eta g g'' + \beta_3 g'' - \beta_4 \eta g''' \quad , \tag{C5}
$$

where

$$
\beta_1 \;=\; \frac{u_s^2 \delta_s'' + u_s'' u_s \delta_s + u_s' u_s \delta_s' - u_s'^2 \delta_s}{u_s u_s' \delta_s' + u_s^2 \delta_s''} \quad \text{and} \quad \beta_2 \;=\; \frac{\frac{u_s^2 \delta_s'^2}{\delta_s} + u_s u_s' \delta_s'}{u_s u_s' \delta_s' + u_s^2 \delta_s''} \quad , \tag{C6}
$$

and where

$$
\beta_3 \;=\; \nu \frac{\frac{u_s \delta_s'}{\delta_s^2} - \frac{u_s'}{\delta_s}}{u_s u_s' \delta_s' + u_s^2 \delta_s''} \quad \text{and} \quad \beta_4 \;=\; \nu \frac{\nu \frac{u_s \delta_s'}{\delta_s^2}}{u_s u_s' \delta_s' + u_s^2 \delta_s''} \quad . \tag{C7}
$$

LIST OF ABBREVIATIONS, ACRONYMS, AND SYMBOLS

ACRONYM	DESCRIPTION
2-D	Two-Dimensional
APG	Adverse Pressure Gradient
FPG	Favorable Pressure Gradient
ODE	Ordinary Differential Equation
PDE	Partial Differential Equation
ZPG	Zero-Pressure Gradient